Differential received power measurements over off-body links for obstruction-resilient pedestrian navigation [Mesure différentielle de puissance reçue sur des liens radios entre corps humain et infrastructure en vue d'une navigation pédestre résiliente aux obstructions]

Bernard Uguen, B. Denis, R. d'Errico, N. Amiot

C. R. Physique 20 (2019) 192–203

Contents lists available at ScienceDirect

Comptes Rendus Physique

www.sciencedirect.com

URSI-France 2018 Workshop: Geolocation and navigation / *Journées URSI-France 2018 : Géolocalisation et navigation*

Differential received power measurements over off-body links for obstruction-resilient pedestrian navigation

Mesure différentielle de puissance reçue sur des liens radios entre corps humain et infrastructure en vue d'une navigation pédestre résiliente aux obstructions

Bernard Uguen [a,*], Benoît Denis [b], Raffaele D'Errico [b], Nicolas Amiot [c]

[a] *Université de Rennes-1, IETR (UMR 6164), Campus de Beaulieu, av. du Général-Leclerc, 35042 Rennes cedex, France*
[b] *CEA–Leti, MINATEC Campus, 17, rue des Martyrs, 38054 Grenoble cedex 9, France*
[c] *Kerlink, 1, rue Jacqueline-Auriol, 35235 Thorigné-Fouillard, France*

ARTICLE INFO

Article history:
Available online 6 June 2019

Keywords:
Wireless body area network
Pedestrian localization
Pedestrian navigation
Differential RSSI

Mots-clés :
Réseaux corporels mobiles
Goniométrie
Localisation et navigation du piéton
Mesure de puissance différentielle

ABSTRACT

In this paper, we aim at improving pedestrian navigation experience based on standard narrow-band wireless technologies and simple radio metrics. The proposed solution takes benefits from body shadowing effects traditionally experienced at body-worn devices, for instance over off-body radio links with respect to fixed elements of infrastructure. The main idea is to infer relative angular information between the carrying body's heading and the received signal's direction of arrival. For this purpose, we consider differential received power measurements with judiciously placed on-body nodes. In comparison with related state-of-the-art contributions, a much lighter on-the-fly self-calibration procedure is made possible, based on the full-scale dynamics of the observed power measurements. We also describe a new algorithm that jointly estimates the body's absolute position and orientation, while benefiting from the body's movement continuity over time. The overall solution is validated by means of field experiments with IEEE 802.15.4-compliant devices operating at 2.4 GHz. Overall, the system is shown to be resilient, not only against self-shadowing effects generated by carrying bodies, but also against occasional obstructions caused by moving pedestrians in the vicinity (e.g., in crowded environments).

RÉSUMÉ

On vise dans cet article à améliorer l'expérience de navigation des piétons basée sur des technologies sans fil standard à bande étroite et une métrique radio simple. La solution proposée tire profit des effets d'ombrage corporel traditionnellement observés sur les dispositifs portés sur le corps, par exemple sur des liaisons radio *off-body* vers les éléments fixes de l'infrastructure. L'idée principale est de déduire des informations angulaires relatives entre le cap du corps porteur et la direction du signal reçu d'arrivée.

* Corresponding author.
E-mail addresses: bernard.uguen@univ-rennes1.fr (B. Uguen), benoit.denis@cea.fr (B. Denis), raffaele.derrico@cea.fr (R. D'Errico), n.amiot@kerlink.fr (N. Amiot).

https://doi.org/10.1016/j.crhy.2019.03.003
1631-0705/

Pour ce faire, nous considérons la puissance logarithmique différentielle reçue avec des nœuds judicieusement placés sur le corps. En comparaison des contributions à l'état de l'art, il est possible de mettre en place un outil beaucoup plus léger de calibrage à la volée. La procédure d'autocalibrage est rendue possible grâce à l'autocalibrage à pleine échelle dynamique des mesures de puissance observées. Nous décrivons également un nouvel algorithme qui estime conjointement la position absolue du corps et son orientation, tout en bénéficiant de la continuité du mouvement du corps dans le temps. La solution globale est validée au moyen d'expériences sur le terrain avec des appareils conformes à la norme IEEE 802.15.4 fonctionnant à 2,4 GHz. Dans l'ensemble, le système s'est avéré résilient, non seulement contre les effets d'auto-occultation générés par les corps porteurs, mais aussi contre les obstructions occasionnelles causées par les piétons qui se déplacent dans le voisinage (par exemple dans des environnements bondés).

1. Introduction

Stimulated by the advent of ultra low power radio and sensor technologies, Wireless Body Area Networks (WBAN) and wearable networks are viewed as key enablers to support a variety of emerging user-centric applications in what is sometimes called the "Internet of Me" (e.g., smart/connected clothing, e-fitness, e-health, and e-wellness, nomadic social networking, personal safety...) [1–3]. Asides, new context-aware mobile services based on physical activity detection or pedestrian navigation in GPS-denied indoor environments have also been put forward recently [4,5].

However, none of the low-cost wireless localization solutions available today can yet offer very high location accuracy regardless of operating conditions, while requiring uniquely a light infrastructure and user-friendly calibration procedures. Accuracy is indeed altered by the combination of uncontrolled device attitude (e.g., leading to unfavorable antenna orientation), electromagnetic perturbations (e.g., caused by the proximity of the carrying hand in case of handset device), strong and systematic body shadowing (e.g., with respect to anchors or base stations) or transient obstructions of the radio links under mobility (e.g., caused by surrounding obstacles or people). These effects are even more critical for wireless localization techniques relying on default Received Signal Strength (RSS) indicators (e.g., typically within non-dedicated narrow-band radio standards such as Zigbee or Bluetooth-LE). The latter do not only suffer from radio irregularities (e.g., non-calibrated Tx power, strong shadowing dispersion...), but they also most often rely on intrinsically parametric approaches. Accordingly, they require the in-site calibration of a priori model parameters or databases, leading to representativeness and reliability issues within both range-dependent path-loss characterization (i.e. statistical) or fingerprinting (i.e. deterministic) techniques. Although fingerprinting approaches are repeatedly promoted for mitigating the effect of body shadowing, the database calibration phase, which requires the collection of RSS fingerprints over multiple positions of a fine spatial grid (and ideally, for multiple discrete orientations of the mobile device), remains tedious, costly and hardly maintainable in practice. Alternative temporal radiolocation metrics such as the time (difference) of arrival usually necessitate much larger bandwidths (e.g., Impulse Radio–Ultra Wideband) and hence, are not yet available within massively deployed narrow-band radio devices. Angle-of-Arrival (AoA) measurements impose the use of antenna arrays at the receiver, leading to additional cost, post-processing, and integration constraints. They are thus usually not considered on the mobile side. In addition, they may strongly suffer from Non-Line-of-Sight (NLoS) situations (i.e. even more significantly than temporal metrics).

In line with recent results on off-body and body-to-body radio channels characterization [6–9], other original initiatives intend to draw benefits from orientation-dependent body shadowing while using standard RSS measurements. In other words, from a localization-oriented perspective, they consider body shadowing as a constructive and deterministic parameter, rather than a random source of nuisance. In [10] for instance, considering back and front on-body RFID readers with respect to a plurality of known tags disseminated in the environment, a path loss model expressed as a function of range and relative body orientation (i.e. the angle between the absolute body orientation and the Rx–Rx line) is injected in a cost function with back and front RSS measurements, enabling the joint non-linear Least Squares (LS) optimization of the body's absolute position and absolute orientation. Alternatively, decoupling the estimation problem, a range-based RSS model is used with average RSS measurements (i.e. averaged over back and front RSS readings) to produce the position estimate first and then, an empirical conditional detection model is considered (i.e. accounting for the probability to detect the tags at the front reader, back reader, or both). This model enables the Maximum Likelihood (ML) estimation of the body's orientation in a second step. Even if heading accuracy levels of about 0.3 rad could be demonstrated in a typical indoor environment, a large number of active tags (on the order of 50) is still required, along with an extensive in-site calibration campaign (i.e. to determine both power path loss and tag detection model parameters). In [11], successive positions estimated through RSS-based fingerprinting by a Viterbi-like tracking algorithm are used to predict the next body's orientation and thus, the corresponding body shadowing induced at a body-worn tag with respect to reference access points. The latter shadowing contributions are then removed from the next RSS observations, based on an orientation-dependent compensation model. Field experiments relying on IEEE 802.15.4-compliant devices at 2.4 GHz show positioning accuracy improvement by about 20%. However, the solution still requires a fingerprinting database, as well as an a priori calibrated compensation model.

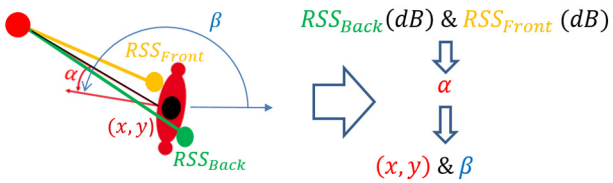

Fig. 1. Exploitation of differential front–back RSSs over off-body links for estimating the body's orientation.

Finally, in [12], the body's relative orientation is first estimated based on differential RSS measurements performed at back and front on-body nodes over off-body links with respect to a few surrounding anchors. These relative measurements then feed an iterative joint estimator of the body's absolute position and absolute orientation, which adopts a linearized Least Squares (LS) matrix form. This solution claims robustness against radio irregularities, obstructions or perturbations over the involved links (e.g., caused by the carrying body or by external obstacles). In addition, it is somehow "less parametric" than the previous techniques due to a much lighter self-calibration procedure, which can be performed on the fly. First experimental validations based on IEEE 802.15.4-compliant devices show that, whereas the body's heading is accurately retrieved, the absolute position still suffers from relatively large errors.

In this paper, we aim at improving significantly position estimates for even better pedestrian navigation experience. In comparison with [12], the main contributions can be summarized as follows: i) we describe a new algorithm that re-injects reliable heading estimates in next estimation steps, thus benefiting from movement continuity over time under typical body mobility (instead of performing static one-shot estimation), without necessitating any a priori state transition model though, ii) we provide a mathematical formalism regarding the disambiguation of relative body angles with an arbitrary number of anchors, as well as the handling of harmful 2π transients, iii) the performance of our joint position and orientation estimator is assessed by means of experimental trials relying on IEEE 802.15.4-compliant devices. On this occasion, we explore further a crowded scenario involving multiple pedestrians so as to illustrate the robustness of the proposed approach against both external obstructions and the dispersion of operating characteristics (i.e. considering the variety of equipped subjects and mobility patterns). In terms of targeted applications, the proposed approach is mainly suitable into harsh indoor navigation contexts, where the environment is particularly obstructed and/or whenever the users can afford wearing smart clothes or at least, non-intrusive on-body devices preserving their freedom of movement (e.g., contrarily to conventional handset-based approaches, which are likely more limited in terms of usage and performance, due to uncontrolled device orientation). Assisting the mobility of vulnerable pedestrians (e.g., blind people or groups of firefighters on the field) is a good example of such applications.

The remainder of the paper is organized as follows. In Section 2, we briefly introduce the problem, as well as the related principles. In Section 3, we describe the overall estimation framework and detail the new proposed algorithmic enhancements. Then Section 4 presents experimental results based on IEEE 802.15.4-compliant integrated devices.

2. General problem statement and concept

Similarly to [10] and [11], the idea consists in benefiting from deterministic orientation-dependent body shadowing effects, which may convey fruitful information for solving the localization problem. In addition to shadowing, assuming mobile on-body nodes and/or mobile scatterers around, small-scale fading also notoriously affects the power received over off-body links due to multipath propagation. In most RSS-based localization scenarios, however, the effects of these rapid power fluctuations are usually mitigated out – to a large extent – by averaging over consecutive measurements. The goal is thus to isolate mostly the range-dependent characteristics of the received power. The size of the averaging window must be judiciously chosen depending on the channel coherence time, given a mobility scenario (e.g., slow pedestrian mobility in our case). As an example, the radio chipsets involved in our experiments [5] give access to the average RSS over the last 8 received modulation symbols.

We herein aim at exploiting the RSS differences (after averaging) observed at a few judiciously placed on-body nodes over off-body (or eventually body-to-body) links so as to estimate the relative angle α formed between the absolute heading direction β of the carrying body (i.e. the absolute orientation with respect to a global reference) and the direction of arrival of the signal received from external nodes. On the other hand, another aim is to avoid requiring any a priori in-site calibrated path loss model, contrarily to [10], for instance. Fig. 1 gives a top illustration of a single mobile user equipped with front and back on-body nodes, which establish off-body radio links with respect to one single external node. If the latter approach is applied with respect to a collection of external nodes set as anchors, one can infer the absolute heading β and the absolute Cartesian coordinates (x, y) of the carrying body (i.e. in a global system), thus covering single-user navigation needs.

In the following, for each equipped body, we will consider a simple configuration with only a few nodes placed on the back and front of a test body, keeping in mind that the described concepts could be easily extended to a larger number of on-body nodes, as well as to other reference on-body locations.

3. Proposed estimation algorithms

3.1. Measurement of the body's relative orientation

Similarly to [12], the relative angle information α is estimated based on a parametric function $map(\gamma)$, also depicted hereafter as angular mapping function, which binds explicitly α with γ, the received power ratio (or power difference in dB) between the RSS levels observed at front and back on-body nodes (with respect to the same external node), namely RSS_{Front} and RSS_{Back}, respectively. For instance, this function can take a polynomial form of arbitrarily high order, whose parameters are either based on a priori models (e.g., knowing an angle-dependent average path loss model, such as that in [8,9]), or even more easily, empirically adjusted to the observed dynamics of γ for each carrying body independently, by means of a light preliminary calibration procedure. As an example, one can just aim at retrieving the minimum and maximum values taken by the received power ratio over (at least) a full rotation of the carrying body, namely $\gamma_{\min} = \min_{t<t_c} \widetilde{\gamma}(t)$ and $\gamma_{\max} = \max_{t<t_c} \widetilde{\gamma}(t)$, with $\widetilde{\gamma}(t)(\text{dB}) = RSS_{\text{Back}}(t)(\text{dB}) - RSS_{\text{Front}}(t)(\text{dB})$, the observed RSS ratio at acquisition time $t < t_c$ up to the calibration time t_c. Accordingly, this calibration can be realized on the fly, without necessitating ground truth orientation information. The mapping function parameters can also be continuously refined as more and more data are collected, thus refining further angular estimates as a function of time.

In the steady-state regime (i.e. after calibration), the relative angle estimate (in radians) is hereafter calculated like in [12] as follows:

$$\widetilde{\alpha} = \frac{\pi(\widetilde{\gamma}(\text{dB}) - \gamma_{\min}(\text{dB}))}{\gamma_{\max}(\text{dB}) - \gamma_{\min}(\text{dB})}. \tag{1}$$

Optionally, the raw RSS ratio can be smoothed by a sliding averaging window before estimating the relative angle. Moreover, more than two on-body nodes can be deployed for better robustness (typically, two front nodes and one back node), giving the opportunity to benefit from diversity and redundancy or to select the best couple of nodes at any time. In this case, after choosing one arbitrary couple as a reference to define the body heading and knowing a priori the deployment of all on-body nodes, it is possible to deliver one single and consistent relative angle estimate over time. For instance, after compensating the known constant angular bias $\Delta\alpha$ between the two couples' directions, one can compute any combination of the two issued relative angles (e.g., as a weighted average). One can also switch from the measurement associated with the reference couple to that of the other selected couple, depending on the context.

3.2. Disambiguation of relative angles

We now assume K elements of infrastructure (anchors) $\{AP_k\}_{k=1\ldots K}$ and 2 (or 3 off-body) radio links per anchor. The unknown body's absolute position (i.e. 2D Cartesian coordinates) and heading are gathered in the state vector:

$$\mathbf{x} = [x, y, \beta]^{\mathsf{T}}$$

The estimated position $M(x, y)$ coincides with the arbitrary origin fixed on the body at the back center node. Each single raw relative angle measurement $\alpha_k^{r|l}(\mathbf{x})$ (according to Sect. 3.1)[1] naturally lies in the interval $[0, \pi[$ rad and, as such, is unsigned:

$$\alpha_k^{r|l}(\mathbf{x}) = \arccos(\hat{\mathbf{p}}_k \cdot \hat{\mathbf{u}}^{r|l}) \tag{2}$$

where $\hat{\mathbf{p}}_k$ is the unitary (normalized) vector originated from the back on-body node and directed to the external anchor A_k and $\hat{\mathbf{u}}^r$ is the unitary (normalized) vector also originated from the back on-body node but co-linear to the reference absolute orientation (e.g., corresponding arbitrarily to the direction binding the back center node to the torso top right node in our experiments), as shown in Fig. 2.

The corresponding disambiguated relative angle $a_k^{r|l}(\mathbf{x})$ expressed in the interval $[-\pi, \pi[$ can be theoretically determined as:

$$a_k^{r|l}(\mathbf{x}) = \text{arctan2}(|\hat{\mathbf{p}}_k \times \hat{\mathbf{u}}^{r|l}|, \hat{\mathbf{p}}_k \cdot \hat{\mathbf{u}}^{r|l}) \tag{3}$$

Orientation angles with respect to anchors are first known in absolute values. Accordingly, $\epsilon_k(\mathbf{x}) = \pm 1$ is fundamentally unknown in the following relation:

$$a_k^r = \epsilon_k(\mathbf{x})\alpha_k(\mathbf{x}) \tag{4}$$

The sign value $\epsilon_k(\mathbf{x})$ can be inferred by exploiting absolute angular values from two additional anchor nodes. The body's motion continuity over time indeed allows us to exploit previous orientation and position information, given the a priori

[1] The notations r and l herein refer to torso top *left* and torso top *right* on-body nodes, respectively; $r|l$ thus indicates that the equation is applicable to both top on-body nodes indifferently.

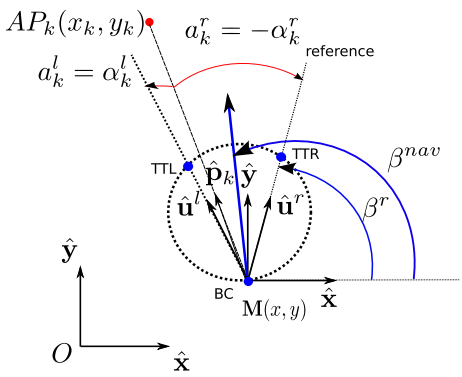

Fig. 2. Joint absolute angle/position estimation problem for a mobile body of 2D coordinates (x, y), relying on $k = 1..K > 1$ fixed elements of 2D coordinates (x_k, y_k) and 3 on-body nodes (back center – BC –, torso top left – TTL – and torso top right – TTR).

knowledge of access points positions (and thus, the knowledge of their spatial ordering with respect to the pedestrian), as follows:

$$\tilde{a}_k^{r|l}(\mathbf{x}) = \text{sign}(\tilde{\alpha}_{m\neq k}^{r|l} - \tilde{\alpha}_{n\neq k}^{r|l})\tilde{\alpha}_k^{r|l} \tag{5}$$

where $m \neq k$ and $n \neq k$ refer to the indexes of the two additional anchor nodes, namely AP_m and AP_n, which have been chosen for being separated in the angular domain from the targeted anchor node AP_k. Note that exploiting 3 off-body links (i.e. 3 on-body nodes) for a given anchor, that is to say, jointly considering lateralized *right* and *left* measurements (e.g., torso top left – back center vs torso top right – back center measurements in our experiments, as shown hereafter), contributes to enhance this disambiguation phase. One can indeed exploit the strong constraint of the known angular separation between *right* and *left* nodes TTL(l) and TTR(r), $\alpha_k^l - \alpha_k^r = \Delta\alpha$. When right and left measurements are exploited in practice, Eq. (5) is actually implemented as

$$\tilde{a}_k^{r|l} = \text{heur}_{t_0}^{r|l}(\tilde{\alpha}_{1,t<t_0}^r, ..., \tilde{\alpha}_{K,t<t_0}^r, \tilde{\alpha}_{m=1,t<t_0}^l, ..., \tilde{\alpha}_{m=K,t<t_0}^l, \Delta\alpha)\tilde{\alpha}_k^{r|l} \tag{6}$$

where the heuristic sign function $\text{heur}_{t_0}^{r|l}()$ takes as arguments all the available contextual information gathered until current time t_0, depending on the particular deployment configuration.

3.3. Joint estimation of the body's absolute position and heading

After determining the set of disambiguated relative angles $\{\tilde{a}_k\}_{k=1..K>1}$ out of received power ratios $\{\tilde{\gamma}_k\}_{k=1..K>1}$ over $2\times K$ off-body radio links with respect to K elements of infrastructure (see Subsections 3.1 and 3.2), we still rely on the known locations of the latter, $\{(x_k, y_k)\}_{k=1..K>1}$, to estimate the body's absolute position and heading, respectively $(\hat{x}, \hat{y})$ and $\hat{\beta}$, as shown in Fig. 3.

The system of non-linear equations to be solved is given by:

$$\begin{cases} \tilde{a}_1 &= \text{arctan2}\left((y_1 - y)\cos\beta - (x_1 - x)\sin\beta, (x_1 - x)\cos\beta + (y_1 - y)\sin\beta\right) \\ \vdots & \\ \tilde{a}_K &= \text{arctan2}\left((y_K - y)\cos\beta - (x_K - x)\sin\beta, (x_K - x)\cos\beta + (y_K - y)\sin\beta\right) \end{cases} \tag{7}$$

is linearized around an arbitrary point $\mathbf{x}^{(n)} = [x^{(n)}, y^{(n)}, \beta^{(n)}]^\intercal$ and solved iteratively, where n refers to the iteration index.

We get the following first-order approximation for each disambiguated relative angle a_k:

$$\delta a_k^{(n+1)} \approx \nabla a_k^{(n)} \cdot \delta\mathbf{x}^{(n+1)}$$

where

$$\delta\mathbf{x}^{(n+1)} = \mathbf{x}^{(n+1)} - \mathbf{x}^{(n)}$$
$$\delta a_k^{(n+1)} = \tilde{a}_k - a_k^{(n)}$$

Practically, this signed angular increment should be kept insensitive to any accidental 2π discontinuity and is, in that respect, implemented as follows:

$$\begin{cases} \delta a_k^{(n+1)} &= \tilde{a}_k - a_k^{(n)} \text{ if } |\tilde{a}_k - a_k^{(n)}| < \pi \\ &= \tilde{a}_k - a_k^{(n)} - 2\pi \text{ if } \tilde{a}_k - a_k^{(n)} > \pi \\ &= a_k^{(n)} - \tilde{a}_k - \pi \text{ if } \tilde{a}_k - a_k^{(n)} < -\pi \end{cases} \tag{8}$$

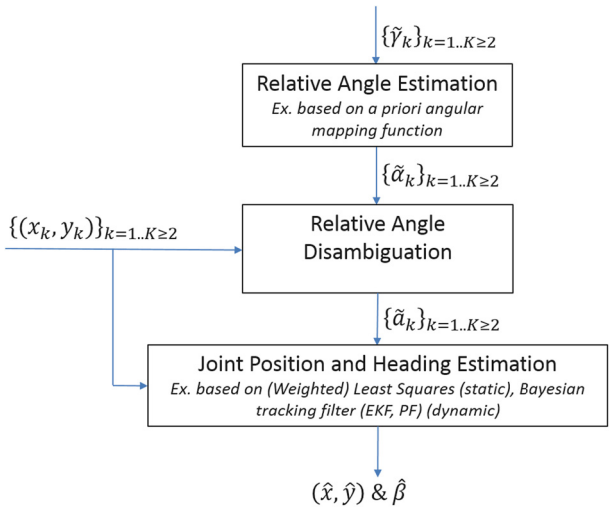

Fig. 3. Procedure for the RSS-based joint estimation of absolute angle β and absolute position (x, y) over body-to-body links with back and front on-body nodes.

Defining the square distance to the k-th anchor as:

$$d_k^{2(n)} = (x_k - x^{(n)})^2 + (y_k - y^{(n)})^2$$

the gradient of $a_k(\mathbf{x})$ is approximated anywhere as the line vector $(1\times\ 3)$

$$\nabla a_k^{(n)} = \nabla a_{k|\mathbf{x}^{(n)}} \approx [\frac{y_k - y^{(n)}}{d_k^{2(n)}}, \frac{x^{(n)} - x_k}{d_k^{2(n)}}, -1]$$

By stacking linewise all the equations corresponding to the K anchors into the $K \times 3$ matrix

$$\mathbf{A}^{(n)} = [\nabla a_{1|\mathbf{x}^{(n)}}; ...; \nabla a_{K|\mathbf{x}^{(n)}}]$$

and forming the $(K \times 1)$ vector involving so-called innovation relative angles (i.e. from n to $n+1$)

$$\mathbf{b}^{(n+1)} = [\delta a_1^{(n+1)} + \nabla a_1^{(n)} \cdot \mathbf{x}^{(n)}, ..., \delta a_K^{(n+1)} + \nabla a_K^{(n)} \cdot \mathbf{x}^{(n)}]^\intercal$$

one can define the one-step pseudo inverse update from the initial guess $\widehat{\mathbf{x}}^{(n)}$ as follows:

$$\widehat{\mathbf{x}}^{(n+1)} = \mathbf{A}^{(n)+}\mathbf{b}^{(n+1)} \tag{9}$$

where $\mathbf{A}^{(n)+}$ is the Moore–Penrose pseudo inverse of matrix $\mathbf{A}^{(n)}$ and substituting $\widehat{\mathbf{x}}^{(n)} \to \mathbf{x}^{(n)}$ in $\mathbf{A}^{(n)}$ and $\mathbf{b}^{(n+1)}$. This equation leads to an iterative joint absolute position and orientation estimator.

3.4. Use of heading information for robust body position tracking

The estimation of position and heading is performed differently depending whether on-body nodes are static or not. In the following, we assume that a dedicated algorithmic block is in charge of determining the static/mobile status, which will be denoted $\phi_m = \{0, 1\}$ in the following.

It turns out that the gradient algorithm presented in Sect. 3.3 is more robust in estimating the heading parameter β. It is thus advantageous under mobility to exploit such heading information as a basis for position prediction (i.e. $\phi = 1$), whereas in the static phase it is preferable to average successive position estimates over time in order to reduce estimation variance through simple coherent integration (i.e. $\phi = 0$), as follows:

$$\hat{\mathbf{p}}[m+1] = \frac{\sum_{k=0}^{N_\mathrm{w}-1} \hat{\mathbf{p}}[m-k] + \hat{\mathbf{p}}_r[m]}{N_\mathrm{w}+1} \left[(1 - \phi_m[m]) + \phi_m[m]\left(1 + \hat{\delta}_m \cdot \hat{\mathbf{u}}^{\mathrm{nav}}[m]\right)\right] \tag{10}$$

where N_w is the averaging window length, $\hat{\mathbf{p}}_r[m]$ is the raw instantaneous position estimate obtained solely from innovation data at time m, while $\hat{\mathbf{p}}[m]$ is the current position estimate taking into account previous position estimates, and

$$\hat{\delta}_m = \hat{\mathbf{p}}_r[m] - \hat{\mathbf{p}}[m]$$
$$\mathbf{u}^{\mathrm{nav}}[m] = [\cos(\beta^{\mathrm{nav}}[m]), \sin(\beta^{\mathrm{nav}}[m])]^\intercal$$

Fig. 4. IEEE802.15.4-compliant HiKoB FOX radio transceivers involved in experimental scenarios 1 and 2.

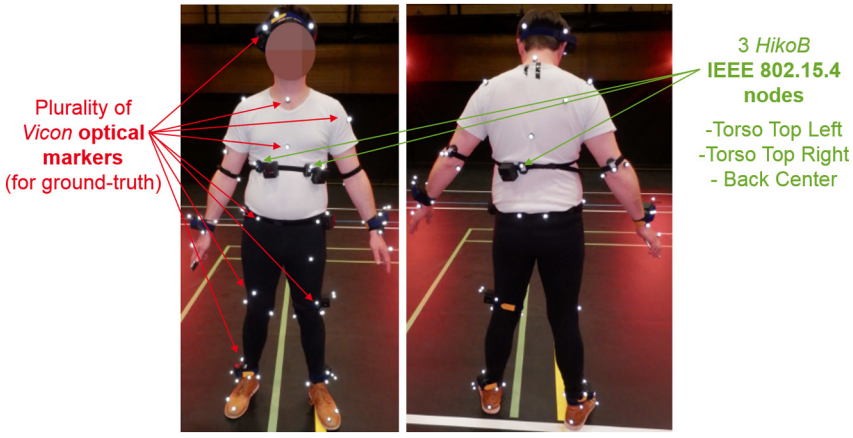

Fig. 5. Front and back pictures of the equipped subject involved in the field experiments, including three on-body *HikoB* radio nodes and tens of on-body *Vicon* optical markers.

with

$$\hat{\beta}^{\text{nav}} \simeq \hat{\beta}^{r} + \frac{\Delta\alpha}{2} \simeq \hat{\beta}^{l} - \frac{\Delta\alpha}{2} \simeq \frac{\hat{\beta}^{r} + \hat{\beta}^{l}}{2}$$

In the static mode, the position is thus simply averaged over N_{w} samples, while in the dynamic mode, the new estimated position is obtained from the last averaged position plus an additional increment projected along the current estimated heading direction. Accordingly, even if this scheme has been kept deliberately simple and does not require any parametric mobility model, it is still expected to take benefit from body movement continuity and space-time correlation, at least to some extent (in terms of both heading and position). Obviously, an extended Kalman filter may provide even more robust performance, but would necessitate the calibration of state noise and transition models under possibly erratic pedestrian mobility. In the results presented hereafter, the raw data time step is $T_{\text{s}} = 0.01$ s and the window size is $N_{\text{w}} = 10$, resulting into a larger sampling period of $N_{\text{w}} \times T_{\text{s}} = 0.1$ s, which still remains compatible with most of real-time applications.

4. Experimental validations

4.1. Experimental set-up and scenarios

We consider the same set-up, scenarios, and data as those accounted for in [12], though focusing more on the joint estimation of the absolute position and orientation (rather than on the estimation of relative orientation), while exploiting further a challenging crowded multi-agent scenario for comparison.

The involved *HiKoB FOX* wireless sensors, which are suited for flexible WBAN tests [13], are compliant with the IEEE 802.15.4 standard in the 2.45 GHz ISM band, giving access to the average RSS indicator over eight received modulation symbols (see Fig. 4). Although up to 12 nodes were deployed on the subject bodies during the full campaign, we herein focus only on three particular on-body nodes, placed at the center of the back (BC) on the one hand, and on the left (TTL) or right (TTR) sides of the torso on the other hand, thus leading to two possible back–front couples of on-body nodes, namely BC-TTL and BC-TTR, and accordingly, to two RSS ratios with respect to each external node (see Fig. 5). In this case, the on-body node accounting for the body location (from the navigation perspective) is chosen as BC. In addition to on-body nodes, $K = 4$ more nodes were also deployed in the environment to serve as fixed anchors, $\{AP_k\}_{k=1\ldots4}$, at the height of approximately 1 m (see Fig. 6).

Besides radio devices, the Oxford Metrics Group's *Vicon* motion capture system [14] was used to deliver high-precision spatial referencing (i.e. seen as ground truth) and accurate synchronization for the deployed on-body nodes. The *Vicon* capture was performed at 100 Hz using 12 infrared cameras surrounding the scene. In each experiment, we equipped the

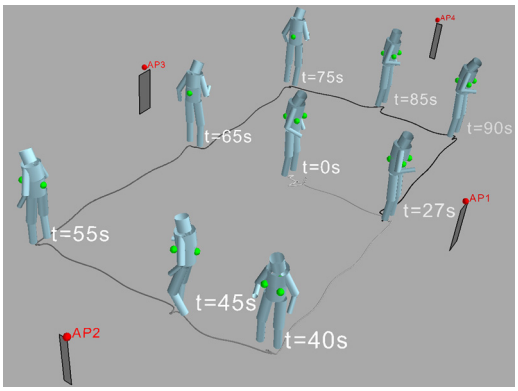

Fig. 6. Partial view of the first physical deployment (Scenario 1), including four fixed anchors (red spheres), the followed trajectory (black ground path), and different time-stamped snapshots of the body poses (articulated chains of light gray cylinders) with on-body radio nodes (green spheres). Despite this snapshot illustration, note that performance evaluation is assessed in a truly dynamic and continuous scenario.

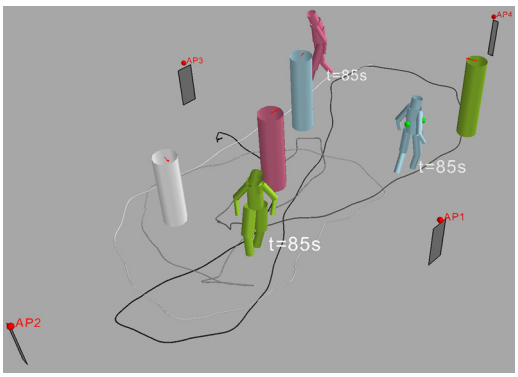

Fig. 7. Partial view of the second physical deployment (Scenario 2), including four fixed anchors (red spheres), three subjects under test (light gray, green and magenta articulated chains of small cylinders), each equipped with three on-body radio nodes (green spheres), and four interfering non-equipped subjects (represented by big cylinders), for a particular time stamp (i.e. 1 snapshot).

test subject with several tens of optical markers placed on the on-body devices and on anatomical landmarks to precisely reconstruct each body segment's 3D position and orientation.

The experiments were realized in a gymnasium dedicated to motion capture studies within a 13 m $\times$ 8 m study area including the four anchors (see Fig. 6) and surrounded by the *Vicon* infrastructure. The considered canonical scenarios deliberately mixed sequences of moderate pedestrian walk and static poses, each trial lasting for about 110 s.

First experimental scenario. In the first series of experiments (Scenario 1), at the beginning of each acquisition, the subject body was standing right in the middle of the scene, facing each anchor for approximately 5 s each and rotating over the four anchors sequentially (i.e. following the same anti-trigonometric sense as that used for anchors labeling and starting with anchor AP_1). Then, at time $t = 20$ s, the subject started moving along a rectangular trajectory centered on the starting point. The sequence is then divided into nine moving sub-sequences, where the subject walks from one point of interest to another, interrupted by nine static sequences, while systematically preserving co-linearity between the sagittal plane and the walking direction. For illustration, Fig. 6 reports time-stamped snapshots of the body postures and orientations at different times spanning from $t = 0$ till $t = 90$ s.

Second scenario. Other experiments have also been conducted in the same test environment with three distinct equipped subjects walking randomly, while gradually increasing the crowd density around. This was realized by involving two additional non-equipped mobile pedestrians every 10 s in the scene (Scenario 2). This scenario was expected to be much more challenging due to the presence of heavy body shadowing transients over off-body links (see Fig. 7).

4.2. Experimental results

In Scenario 1, Fig. 8 shows the time evolution of ground-truth space increments (in absolute value) of the average body position, $||\mathbf{p}(m+1) - \mathbf{p}(m)||_2$, along with the resulting mask function $\phi_m[m]$, which indicates the position of a mobile or static body. For mobility detection, we consider a simple threshold crossing strategy with hysteresis. Accordingly, one can

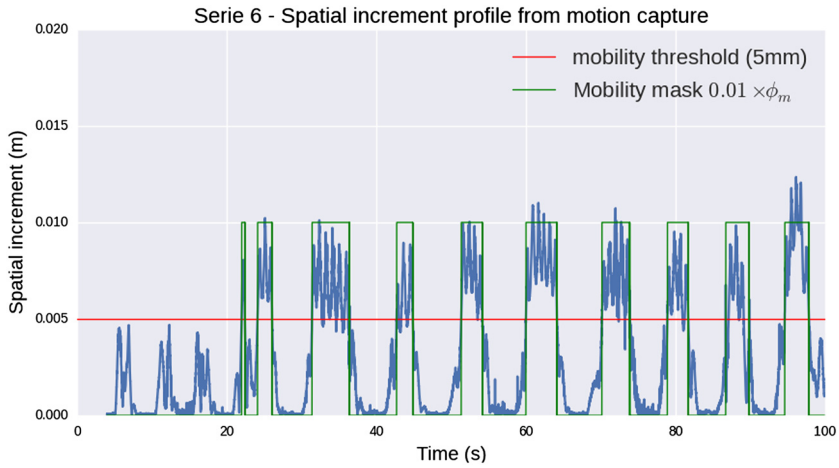

Fig. 8. Mobility status (green) extracted from ground-truth spatial increments (blue) as a function of time, based on threshold (red) crossing in Scenario 1. For the first part of the recording, the body is rotating. Accordingly, only the heading is changing while the position remains roughly static.

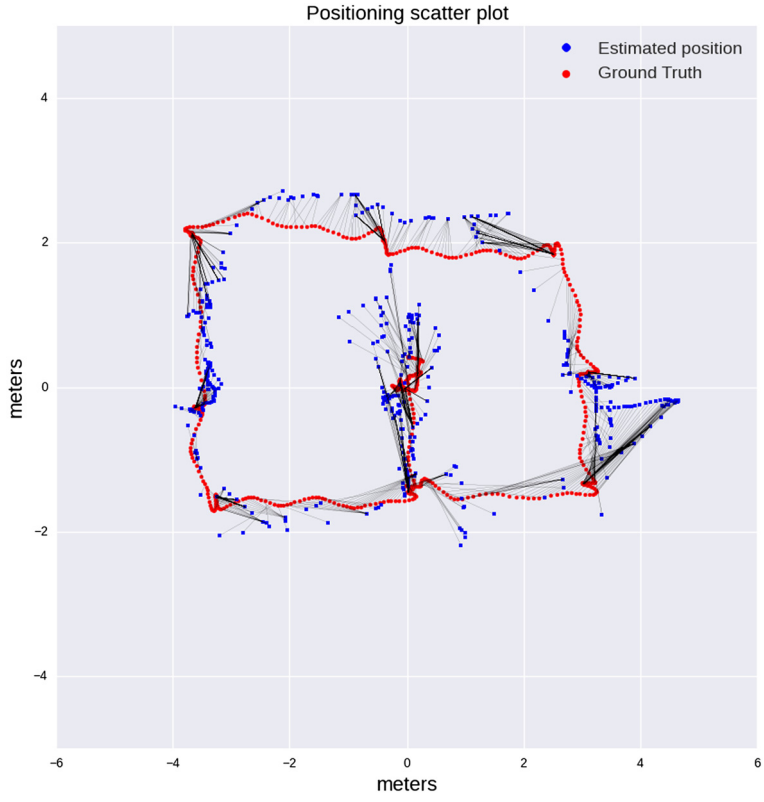

Fig. 9. Positioning scatter plot over the entire trajectory in the single-user case (Scenario 1).

prevent from false alarms caused by micro-mobility effects (as shown before 20 s in our example, as the body is rotating while keeping the same position), as well as from immediate triggering down and thus, mobility missed detection, once the indicator is in the *up* mobile state. An additional duration criterion is also applied specifically to *up* mobile states to avoid false alarms triggered on too spurious signals (i.e. as shown around 22 s on the illustrated example). Finally, it is clearly seen that typical space increments are practically bounded by $\delta_{\max}$ under typical pedestrian mobility, thus justifying the approach taken in Eq. (10). In our algorithm, such mobility detection can be easily implemented based on the sequence of estimated positions.

Fig. 9 shows the scatterplot (blue dots) of the estimated trajectory superposed with the actual trajectory (red dots). Estimated and actual positions are connected by a thin black segment, accounting for the estimation error. Note that these

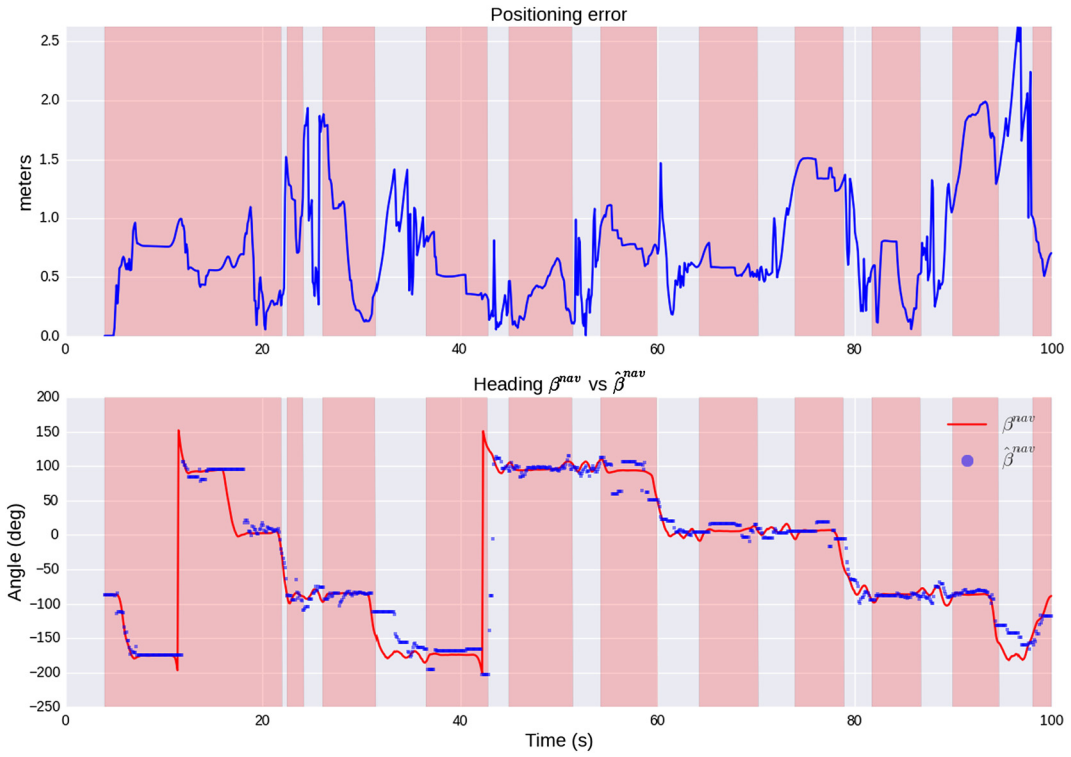

Fig. 10. Positioning error vs time (top), estimated and true heading versus time (bottom), both in the single-user case (Scenario 1) where static portions of time are shaded in pink.

results have been obtained without applying any extra Bayesian tracking on top of the positioning step. Fig. 10 shows the time evolution of the corresponding positioning error, as well as the time evolution of both true and estimated heading.

Fig. 11 shows the empirical Cumulative Density Function (CDF) of the body position estimation error in Scenario 1 for the proposed algorithm exploiting both mobility status and re-using the heading information from one iteration to the next, in comparison with the simpler joint estimation algorithm initially introduced in [12]. When using neither averaging nor mobility status information, median and worst-case positioning errors of about 1.1 m and 3.7 m can be observed. With the new proposed algorithm, median and worst-case positioning errors of about 0.7 m and 2.6 m are achieved (i.e. leading to relative gains of 39% and 28%, respectively). These results demonstrate the utility of exploiting the estimated body heading information, which is robust at any time, as shown in Fig. 10, thus being globally beneficial to the joint estimation process.

As for the second scenario, Fig. 12 and Fig. 13 show the instantaneous position and heading estimation errors as a function of time and the empirical CDF of positioning errors within the second scenario, respectively. The performance degradation (e.g., a median position error on the order of 1 m) looks reasonable in comparison with the single-user case, considering how crowded the scene is. This illustrates by means of real experimental data the resilience of the proposed solution in case of generalized radio link obstructions generated by both self-body shadowing and external obstacles (including other pedestrians in the vicinity).

5. Conclusion

In this paper, we have described a very simple pedestrian navigation solution relying on differential RSS measurements performed at on-body nodes with respect to external nodes (i.e. over off-body and/or body-to-body links), benefiting from stable heading information over time. This approach has been validated by means of real field experiments, relying on IEEE 802.15.4-compliant integrated devices. The proposed scheme has been shown to be fairly robust against both body shadowing and external obstructions of the off-body links (e.g., caused by other moving pedestrians), with typical median errors below 1 m. This makes the solution very promising in challenging environments such as indoor and/or crowded public spaces.

Future works will aim at determining optimal inference schemes for better disambiguation of relative angles (instead of the currently adopted heuristic scenario-dependent rules) and better handling of 2π angular transients, thus mitigating false alarms triggered by noisy input angle measurements. In addition, the proposed approach shall be extended into cooperative tracking scenarios, relying on body-to-body radio links (i.e. on top of off-body links) and a priori mobility models to capture even better the space-time correlation of both body and group movement patterns through filtering (e.g., with Extended Kalman or particle filters).

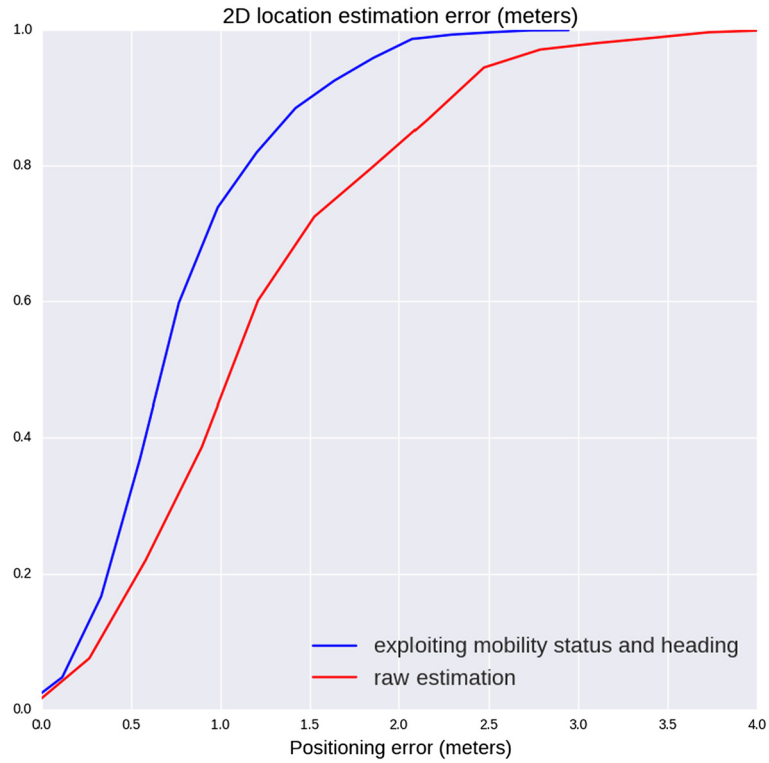

Fig. 11. Empirical CDF of positioning error over the entire trajectory in the single-user case (Scenario 1), exploiting mobility status and heading (blue) or raw joint estimation from [12] (red).

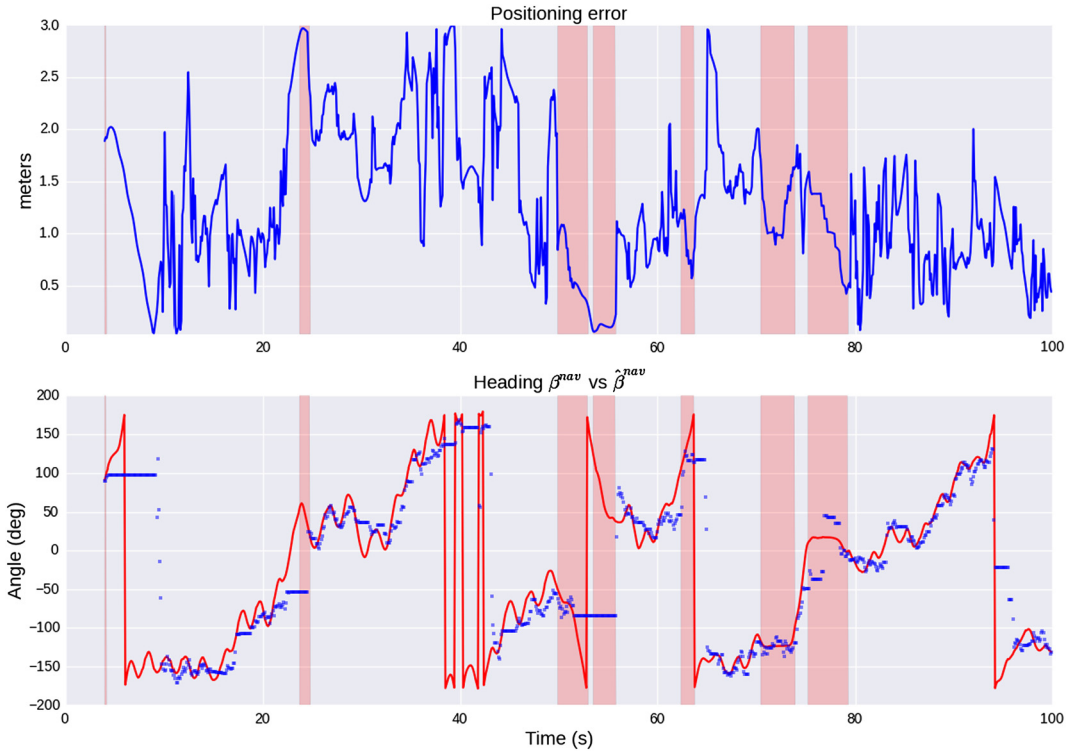

Fig. 12. Positioning error vs time (top) and estimated and true headings vs time (bottom), both in the multi-user case (Scenario 2).

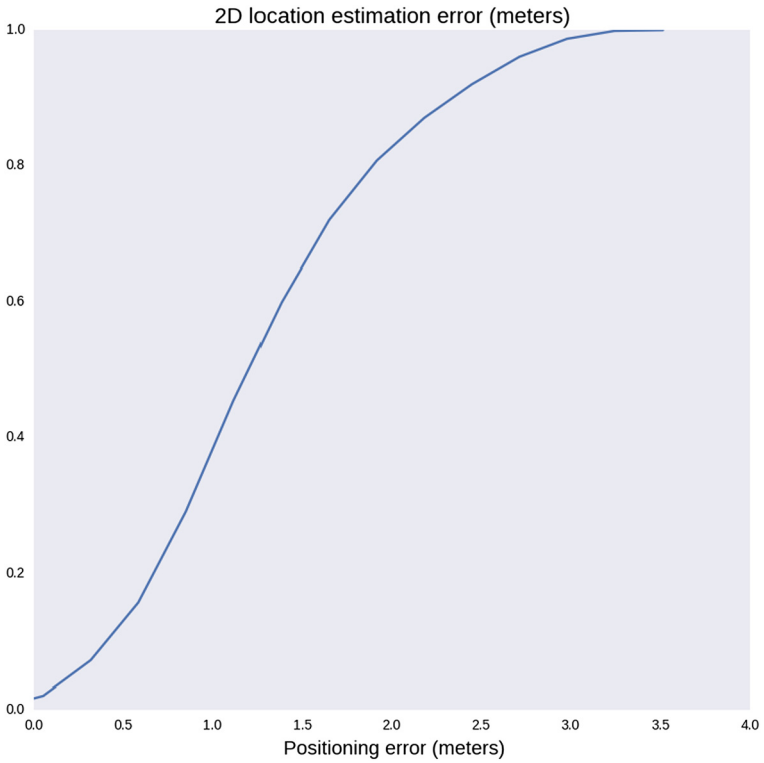

Fig. 13. Empirical CDF of positioning error over the entire trajectory in the multi-user case (Scenario 2).

References

[1] S. Movassaghi, M. Abolhasan, J. Lipman, D. Smith, A. Jamalipour, Wireless body area networks: a survey, IEEE Commun. Surv. Tutor. 16 (3) (2014) 1658–1686.
[2] M. Maman, B. Denis, R. D'Errico, Research trends in wireless body area networks: from on-body to body-to-body cooperation, in: Proc. ISMICT'14, April 2014.
[3] C.C.Y. Poon, B.P.L. Lo, M.R. Yuce, A. Alomainy, Y. Hao, Body sensor networks: in the era of big data and beyond, IEEE Rev. Biomed. Eng. 8 (2015) 4–16.
[4] S.C. Mukhopadhyay, Wearable sensors for human activity monitoring: a review, IEEE Sens. J. 15 (3) (March 2015) 1321–1330.
[5] B. Denis, N. Amiot, B. Uguen, A. Guizar, C. Goursaud, A. Ouni, C. Chaudet, Qualitative analysis of RSSI behavior in cooperative wireless body area networks for mobility detection and navigation applications, in: Proc. IEEE ICECS'14, Bordeaux, France, 9–12 December 2014, pp. 834–837.
[6] R. Rosini, R. D'Errico, Off-body channel modelling at 2.45 GHz for two different antennas, in: Proc. EUCAP'12, Prague, 26–30 March 2012, pp. 3378–3382.
[7] R. Rosini, R. Verdone, R. D'Errico, Body-to-body indoor channel modeling at 2.45 GHz, IEEE Trans. Antennas Propag. 62 (11) (2014) 5807–5819.
[8] F. Mani, R. D'Errico, A spatially aware channel model for body-to-body communications, IEEE Trans. Antennas Propag. 64 (8) (2016) 3611–3618.
[9] M. Maman, F. Mani, B. Denis, R. D'Errico, Coexistence evaluation of multiple wearable networks based on realistic on-body and body-to-body channel models, in: Proc. ISMICT'16, 2016.
[10] F. Seco, A.R. Jiménez, F. Zampella, Joint estimation of indoor position and orientation from rf signal strength measurements, in: International Conference on Indoor Positioning and Indoor Navigation, Montbéliard–Belfort, France, 28–31 October 2013, pp. 1–8.
[11] J. Trogh, D. Plets, L. Martens, W. Joseph, Improved tracking by mitigating the influence of the human body, in: 2015 IEEE Globecom Workshops (GC Wkshps), 6–10 December 2015, San Diego, CA, USA, pp. 1–6.
[12] B. Denis, B. Uguen, F. Mani, R. D'Errico, N. Amiot, Joint orientation and position estimation from differential RSS measurements at on-body nodes, in: 27th IEEE International Symposium on Personal Indooor Mobile radio Communications 2016 (IEEE PIMRC'16), Valencia, Spain, 4–7 September 2016.
[13] M. Lauzier, P. Ferrand, A. Fraboulet, H. Parvery, J.M. Gorce, Full mesh channel measurements on body area networks under walking scenarios, in: Proc. EuCAP'13, Gothenburg, Sweden, 8–12 April 2013, pp. 3508–3512.
[14] B. Bideau, R. Kulpa, N. Vignais, S. Brault, F. Multon, C. Craig, Using virtual reality to analyze sports performance, IEEE Comput. Graph. Appl. 30 (2) (2010) 14–21.